Title: *Characterizing Delamination Migration in Carbon/Epoxy Tape Laminates for* Proceedings of the **American Society for Composites – Twenty-Seventh Technical Conference**

Authors: James G. Ratcliffe[1]
Michael W. Czabaj[2]
T. Kevin O'Brien[2]

[1] National Institute of Aerospace, Hampton, VA. Resident at Durability, Damage Tolerance, and Reliability Branch NASA Langley Research Center, Hampton, VA 23681

[2] Durability, Damage Tolerance, and Reliability Branch NASA Langley Research Center, Hampton, VA 23681

ABSTRACT

A new test method is presented for the purpose of investigating migration of a delamination between neighboring ply interfaces in fiber-reinforced, polymer matrix tape laminates. The test is a single cantilever beam configuration consisting of a cross-ply laminate with a polytetrafluoroethylene (PTFE) insert implanted at the mid-plane and spanning part way along the length of the specimen. The insert is located between a 0-degree ply (specimen length direction) and a stack of four 90-degree plies (specimen width direction). The specimen is clamped at both ends onto a rigid baseplate and is loaded on its upper surface via a piano hinge. Tests were conducted with the load-application point located on the intact portion of the specimen in order to initiate delamination growth onset followed by migration of the delamination to a neighboring 90/0 ply interface by kinking through the 90-degree ply stack. Varying this position was found to affect the distance relative to the load-application point at which migration initiated. In each specimen, migration initiated by a gradual transition of the delamination at the 0/90 interface into the 90-degree ply stack. In contrast, transition of the kinked crack into the 90/0 interface was sudden. Fractography of the specimens indicated that delamination prior to migration was generally mixed mode-I/II. Inspection of the kink surface revealed mode-I fracture. In general, use of this test allows for the observation of the growth of a delamination followed by migration of the delamination to another ply interface, and should thus provide a means for validating analyses aimed at simulating migration.

INTRODUCTION

Since their introduction as material systems in aerospace vehicles, fiber-reinforced polymer matrix composite tape laminates are known to suffer from life-limiting delamination [1]. This tendency to form delaminations and the difficulty in

detecting such damage, has historically limited the use of these material systems in safety critical (primary) structure [2]. In an attempt to reverse this scenario, delamination has received considerable attention in the research community. In particular, a significant amount of attention has been paid to characterizing the three modes of delamination (including delamination under mixed mode loading), which has resulted in testing methods for evaluating fracture toughness and fatigue behavior associated with these delamination modes [3-11].

Delamination simulation is currently being included in commercial finite element analysis (FEA) codes based on either a virtual crack closure technique [12, 13] or a cohesive zone model [14-17]. These analyses are driven by fracture parameters measured using characterization tests. While this overall approach significantly enhances the capability of simulating delamination growth, the vast majority of research has focused mainly on delamination confined to a single ply interface. In reality, damage in composite laminates often involves delaminations that migrate between different ply interfaces. Two such examples that are well documented in the literature include, 1) the classic spiral stair case configuration of delaminations formed after an impact event that arises due to migration of delaminations through several ply interfaces [18-19] and 2) debonding between the flange and skin of integrally stiffened panels that has been shown to involve significant delamination migration [20-21]. These examples highlight that knowledge of delamination growth alone is insufficient for being able to simulate some of the key progressive damage mechanisms that potentially limit the use of composite laminates in aerospace structure. Furthermore, work has shown that simulation of damage formation (including delamination migration) in relatively simple element specimens such as open-hole tension specimens is difficult to achieve with currently established analysis tools [22].

Partly in recognition of these difficulties, recent work has focused on developing fracture tools for use in commercial FEA codes [23-24], which build upon a numerical framework that enables simulation of fracture whose path is not necessarily confined to element boundaries [25]. While these newly developed tools, known generically as extended and augmented finite element methods (X-FEM and A-FEM), permit the simulation of events such as delamination migration, precise criteria for establishing the occurrence of this process are not well understood. Analytical methods based on energy considerations have been developed for predicting the kinking of interface cracks (a process directly analogous to migration, which involves an interface crack turning and propagating into one of the interfacing materials) for isotropic [26] and orthotropic [27] materials. However, these kinking criteria to date have not been commonly applied to delamination migration problems.

Although previous tests have been able to clearly document delamination migration, they may not be ideally suited for pinpointing the precise conditions under which delamination migration initiates, due either to multiple damage events taking place [20] or the relatively complex test configuration [28]. Consequently, it follows that these tests may not be ideal means of evaluating kinking criteria for methods such as X-FEM.

The objective of this work was to directly address the issue stated above and to develop a testing method that focuses on the delamination migration process. To this end, a single cantilever beam (SCB) specimen comprised of a IM7/8552

graphite cross-ply tape laminate was designed. The specimen, illustrated in Figure 1, contains a polytetrafluoroethylene (PTFE) insert implanted at the mid-plane and spanning part way along the length of the specimen. Specimens are loaded in such a manner as to result in delamination growth onset followed by migration of the delamination to another ply interface. The use of a cross-ply laminate allows an approximately two-dimensional characterization of a single migration event. This provides an opportunity to evaluate analytical methods aimed at simulating migration and may help identify appropriate kinking criteria. This test also offers the opportunity for distinguishing between the migration behavior of various composite material systems.

The remainder of this paper details the design of the SCB specimen, describes the tests conducted and concludes with a presentation of the test results with accompanying discussion.

SCB DELAMINATION MIGRATION TESTS

SCB Specimen and Fixture

SPECIMEN CONFIGURATION

A new test method was developed that is based upon the single cantilever beam configuration illustrated in Figure 1. The specimen design possesses three main features that permit the controlled observation of delamination growth followed by migration to another ply interface. First, the specimen geometry is in the form of a beam with the intent of promoting uniform delamination growth and migration across the specimen width. Second, the specimen contains a PTFE insert (acting as an artificial delamination) at an interface between a 0-degree ply (specimen span direction) and a stack of four 90-degree plies (specimen width direction). This provides an opportunity for the delamination to migrate to another ply interface by kinking through the 90-degree ply stack. Third, the specimen can be loaded in a manner to cause delamination growth from the PTFE insert that eventually migrates to another ply interface. This sequence of fracture events (illustrated in Figure 2) is made possible by the way in which specimen loading affects shear stresses acting across the delamination front.

The following three sections contain a detailed description of the steps taken in designing the specimen.

STACKING SEQUENCE AND DIMENSIONS

The first step to design the SCB specimen was to identify a stacking sequence that allows for migration of the delamination to another ply interface. A cross-ply stacking sequence was selected in order to promote migration uniformly across the specimen width. As shown in Figure 1, the specimen consists of three regions corresponding to the two sublaminates in the delaminated portion of the specimen and the intact portion of the specimen. The three regions of the specimen are labeled in Figure 1 using numbers such as ①.

The SCB specimen is cut from a 44-ply laminate that is a slight modification to a symmetric laminate as shown in Figure 3. The nominal total thickness of the 44-ply specimens is 5.25mm, corresponding to a 0.12mm ply thickness. One of the 0-degree plies in this stacking sequence was relocated to interface with the PTFE insert as illustrated in Figure 3. This 0/90 ply interface will be the first to delaminate during a test. A second 0-degree ply was also relocated as illustrated in Figure 3 in order to help minimize the asymmetry of the lower arm portion of the specimen.

A laminated plate theory analysis [29] was performed in order to evaluate the coupling stiffness values that arise from the slight asymmetry of the specimen. The analysis showed that in both the lower sublaminate and intact regions of the specimen all coupling terms are zero except for the extension-bending coupling, $B_{11,}$ which was small relative to the corresponding terms in the A and D matrices. The upper sublaminate is balanced and symmetric, and hence, exhibits no coupling stiffness values.

Specimen length (L_s=115mm) was chosen to result in a beam short enough to easily fit into a small tabletop load frame. Specimen width (B=12.7mm) was chosen in order to promote plane strain loading conditions in the specimen while maintaining a wide enough specimen to mitigate edge effects. Each specimen also contained an initial delamination length (a_0 as defined in Figure 1) of 49mm. A strength of materials analysis was performed to assess the likelihood of arm failure during a test and found that such failure would not be likely.

SCB TEST FIXTURE

The SCB test fixture is pictured in Figure 4 and was designed to enable adjustment of the specimen location along the span direction and also ensure precise alignment with respect to the fixture. Fixturing was also required to enable clamping of both ends of the specimen (as seen in Figure 4). The lower portion of the fixture consists of a grooved steel baseplate that is threaded directly into the test machine load cell (denoted as lower baseplate in Figure 4). A second steel plate (denoted as upper baseplate in Figure 4) mates with the baseplate using a tongue and groove type of connection. The SCB specimen is clamped at both ends to the second plate as shown in Figure 4. Holes were drilled and threaded in the upper baseplate along the span direction, and shoulder screws were used as guide pins to enable precise specimen alignment (the holes are indicated in Figure 4). These screws were removed prior to each test once the specimen was securely clamped into the fixture. The specimen position along its length direction can be adjusted by sliding the upper baseplate over the lower baseplate, which is performed to ensure proper alignment of the piano hinge bonded to the specimen with the loading rod (see Figure 4). An array of four bolts secures both plates to each other, preventing further sliding during a test. Load is applied to a specimen via the 12.7mm-long piano hinge pictured in Figure 4. The load is applied to the specimen through a 300mm-long rod that is hinged at both ends. The top end is connected to the machine crosshead. The long loading arm minimized the introduction of horizontal loading that would otherwise accumulate as the specimen deforms. This method of mitigating horizontal loading is preferable over other methods, such as setting the

baseplates on a moveable carriage, because fixture mass is minimized, making the entire apparatus more suitable for cyclic loading.

The compliance of the test fixture was measured by loading a 12.7mm-wide, 6.35mm-thick steel bar that was clamped into the SCB fixture. The specimen was loaded up to the maximum force observed during actual SCB tests (350N) at the mid-span via the same piano hinge configuration described previously. The fixture compliance was then computed by subtracting the compliance of the steel bar (computed using beam theory) from the compliance measured during the test. The fixture compliance was found to be 365×10^{-6}mm/N, which was approximately 10% of the compliance of the SCB specimen that exhibited the smallest compliance. Although this relatively significant fixture compliance does not affect the observations made during the SCB tests, specimen deformation at the load-application point was indicated by the crosshead displacement of the load frame, and hence, analyses conducted to simulate these tests should account for the fixture compliance.

SPECIMEN LOAD INTRODUCTION

The load-application point on each specimen was positioned a distance, L, from the edge of the test fixture clamp as indicated in Figure 1. The distance, L, (also referred to as the 'load offset') was set to be greater than or equal to the initial delamination length, a_0 (Figure 1). This load-offset range was chosen to promote delamination growth onset followed by migration of the delamination to a different ply interface. This was achieved by considering the following hypothesis.

As the specimen is loaded (Figure 2a), the opening deformation in the vicinity of the PTFE insert front is coupled with the corresponding shear stress acting across it. This coupling mainly arises from the geometry of the SCB specimen. However, the mismatch in bending stiffness of the 0-degree ply and stack of four 90-degree plies below and above the PTFE insert, respectively, also contributes to this coupling. In the case of the loading configuration illustrated in Figure 2a (delamination length less than the load offset, i.e. $a/L < 1$), the shear stress acting across the PTFE insert front promotes kinking of the delamination towards the baseplate side of the specimen. However, the 0-degree ply below the PTFE insert prevents this from occurring, and instead, delamination grows along the 0/90 ply interface.

The delamination continues to propagate along the 0/90 interface and grows past the load-application point (such that $a/L > 1$, Figure 2b), eventually leading to a reversal of the sign of the shear stress acting across the delamination front. The shear stress now promotes kinking of the delamination into the 90-degree ply stack towards the loaded side of the specimen, which will occur once it is energetically favorable to do so. According to He and Hutchinson [26], this will occur when the following inequality is satisfied:

$$\frac{G_k}{G_{Ic}} > \frac{G}{G_c} \tag{1}$$

Where G_k is the maximum strain energy release rate for the kinked crack with respect to the kink angle, Ω (see Figure 2). The parameter G_{Ic} is the mode-I critical strain energy release rate of the material through which the kinked crack propagates

(in this case the 90-degree ply stack). The parameters G and G_c are the strain energy release rate at the interface crack (in this case the 0/90 delamination) and the critical strain energy release rate at the interface, respectively. This analytical treatment is for isotropic solids, but in the case of the SCB specimen, is expected to act as a reasonable guide because the 90-degree ply stack is transversely isotropic.

The kinking crack will eventually propagate through the entire 90-degree ply stack and will transition into the interface between the ply stack and neighboring stack of three 0-degree plies, thereby completing the migration process.

A series of finite element analyses were conducted in order to help corroborate the aforementioned hypothesis. Specimen dimensions used in the analyses are presented in Figure 5. Eleven analyses were performed, each with the specimen loaded at the mid-span but containing different delamination lengths, as illustrated in Figure 5. The analyses were conducted using the commercial code, ABAQUS®[3]/Standard version 6.11 [30]. Solid, eight-node brick elements (ABAQUS® type C3D8i) were used to represent the specimen. A composite layer option was used to represent specimen stacking sequence, whereby one layer of elements was used to represent one or more plies. In this case, the orthotropic ply properties [31] (see TABLE I for properties used in this analysis) were oriented according to the specimen stacking sequence. The 0/90 delamination was modeled by including elements with coincident nodes on the plane of the delamination. A fine mesh was used in the vicinity of the delamination front to accommodate for the rapid change in strain field. The element thickness at the delamination front (in the x and z-axes) was one ply thickness. A similar meshing technique was adopted during an analysis of a double cantilever beam specimen [32]. An additional rectangular mesh was positioned in the location corresponding to the plate of the piano hinge. The hinge was represented as a linear-elastic isotropic material with standard properties of aluminum. Boundary conditions applied to the model are illustrated in Figure 5. Load application was simulated by prescribing a fixed displacement of 0.5mm in the z-direction along the row of nodes located at the point indicated in Figure 5. The same prescribed displacement was applied in each model in order to mimic the displacement-controlled condition of the actual SCB tests. Coupled thermo-mechanical analyses were performed in order to capture the thermal residual stresses arising from the cure of the slightly non-symmetrical laminate (a total temperature gradient of 180^{o}C was assumed. The coefficients of thermal expansion assumed for IM7/8552 are listed in TABLE I). After each analysis run, the deformed region local to the delamination front (in the xz-plane) was observed and the sign of the shear deformation was recorded.

The components of the strain energy release rate, G_I, G_{II}, and G_{III}, (average across the delamination front) were computed using VCCT [12,13] for each of the eleven delamination lengths. In each case, the crack tip element length was kept constant. Hence, although the strain energy release rate components are non-convergent [33], the overall effect of delamination length on these values is assumed to be accurate. The mode-II strain energy release rate as a percentage of the total strain energy release rate, G_{II}/G_T (where $G_T=G_I+G_{II}+G_{III}$), is plotted in Figure 6 as a function of normalized delamination length, a/L. The plot shows that G_{II}/G_T oscillates in magnitude with a minimum close to zero at delamination

[3] ABAQUS® is manufactured by Dassault Systèmes Simulia Corp. (DSS), Providence, RI, USA.

lengths just greater than the load offset. It was noted that the shear stress acting across the delamination front would tend to favor delamination growth when a/L was less than or equal to 1.05, as illustrated in Figure 6. The values of G_{II}/G_T at which this was the case are plotted as open symbols and connected by a dashed line. At delamination lengths greater than the load offset (a/L > 1.05), the shear stress acting across the delamination front changed in sign to favor kinking of the delamination into the 90-degree ply stack, as illustrated in Figure 6. The values of G_{II}/G_T at which this was the case are plotted as closed symbols connected by a solid line. Overall, the analysis results indicate that G_{II}/G_T diminishes to zero as the sign of shear stress reverses, and the conditions (shear stress sign) necessary to favor migration will occur when the delamination length is greater than 1.05L. Thus, the findings appear to corroborate the hypothesis that the occurrence of migration can be controlled by the position of the load-application point on the SCB specimen.

Specimen Manufacture and Materials

A 300mm-square plate of IM7/8552 tape laminate was laid up with the stacking sequence described earlier. A 127mm-wide strip of 12μm-thick PTFE was positioned across the plate between plies 22 and 23. The plate was cured in a hot press oven using the cure cycle suggested by the composite material manufacturer [34]. Upon completion of the cure cycle, a 12.5mm-wide strip was cut from each side of the plate and 42 specimens were cut. A 15mm-long strip was cut from the end of the upper sublaminate of each specimen using a 0.4mm-diameter diamond wire, creating a protruding lip that was clamped during the SCB tests (this lip is illustrated in Figure 1 under the left-hand clamp). A 0.02mm-thick metal shim was positioned along the delamination in the cut region to protect the neighboring specimen arm material as the saw approached the end of the cut. Specimens were stored in a desiccator for a period of approximately two months prior to testing.

SCB Tests

Prior to testing, the edges of all specimens were polished to enable detailed examination of the plies under an optical microscope. Measurements of specimen width and thickness were then taken. The sides of each specimen were then coated with a thin layer of white paint to highlight the delamination and migration events as viewed from the sides of each specimen during a test.

Specimens were loaded with four different load offsets (Figure 1), namely, $L=a_0$, $1.1a_0$, $1.2a_0$, and $1.3a_0$ (where a_0=49mm). Four repeat specimens with load offsets equal to $L=a_0$, $1.1a_0$, $1.2a_0$, and $1.3a_0$ and three repeats with a load offset of $1.3a_0$ were tested, resulting in a total of 15 specimens.

The SCB tests were conducted using a servo-hydraulic test machine equipped with a 450N load cell. Specimens were placed into the SCB test fixture such that contact was made with both guide pins, ensuring precise specimen alignment. The specimens were secured to the upper baseplate of the test fixture via clamps at both ends. Three bolts secured the clamps and were tightened to a torque of approximately 900N-mm. After proper alignment was established with the

specimen length perpendicular to the hinge axis, specimens were loaded under displacement control at a rate of 0.127mm/min in the direction indicated in Figure 1. Specimens were unloaded at the same loading rate. Applied load, *P*, and crosshead displacement, *d* (referred to as displacement in remainder of paper), were recorded throughout each test. Delamination growth and migration was recorded by viewing both sides of each specimen using a pair of cameras equipped with macro lenses. Images of the delamination and migration events were recorded as they occurred during a test. The cameras were synchronized with the force and displacement output collected by the data acquisition system, enabling documentation of the exact force and displacement associated with each image.

Post-Test Inspection

After the completion of a test, both edges of the specimen were cleaned with alcohol to remove the white paint. The delamination and migration paths as viewed from both edges were inspected using an optical microscope at a 40-80X-magnification level. Specimens were then split along the existing delamination plane in order to confirm the PTFE insert front location. The fracture surfaces of a selection of specimens tested using each of the four load offsets were also inspected using a Philips XC30 scanning electron microscope.

RESULTS / DISCISSION

SCB Specimen Response and Fracture Events

LOADING COINCIDENT WITH PTFE INSERT FRONT

The force/displacement responses of the four specimens with $L=a_0$ are shown in Figure 7. As can be seen, the response of the specimens was very consistent. This was also true for the overall sequence of fracture events observed in each specimen. Included in Figure 7 are images of the events that were observed at various key moments during a test. The overall sequence of events was as follows: 1) Specimens responded linearly to loading up to some critical force, 2) an unstable event took place once this critical force was reached. This event included unstable delamination growth that either arrested just prior to the onset of migration or began migrating through the upper 90-degree ply stack to be arrested part way through the stack. Total delamination growth prior to migration ranged between 8 and 9mm, 3) loading of the specimens was continued (all specimens appeared to respond elastically at this stage) until a second critical force at which point a second unstable event occurred. This event involved migration of the delamination via a kinking crack through the upper 90-degree ply stack. Further loading resulted in stable growth of the migrated delamination, 4) specimens responded linearly to unloading, and exhibited a residual displacement of approximately 0.12mm

Inspection of the specimen edges under an optical microscope indicated that after growth onset from the PTFE insert, the delamination grew directly along the 0/90 interface for approximately 1mm after which point the delamination seemed to

transition into the lower 0-degree ply (see circled number 1 in Figure 8). This transition into the 0-degree ply, however, is likely only a free surface edge effect because as will be shown in a later fractographic examination of the delamination surface, no evidence of migration into the 0-degre ply was observed. The delamination appeared to skim the top of the 0-degree ply until just prior to migration, at which point the delamination appears to transition more to the 90 ply side of the interface (see circled number 2 in Figure 8) and gradually kinks through the upper 90-degree ply stack. Upon initial consideration, this observation seems to contradict the argument put forward in the previous section concerning load introduction, where it was postulated that the lower 0-degree ply will confine delamination growth prior to migration exactly to the 0/90 interface. This argument is thought to still hold, however, and the observed growth path is explained by the fact that fibers in the 0-degree ply are not parallel and perfectly aligned along this direction. This provides an opportunity for cracks to grow between misaligned fibers, particularly when the shear stress (Figure 2a) promotes kinking of the delamination through the lower 0-degree ply. Evidence of this occurrence was also found during the fractographic analysis presented later in the paper. As it is still energetically unfavorable for the delamination to completely kink through the 0-degree ply, delamination proceeds near the 0/90 interface. As the delamination grows further, the shear stress changes sign, favoring kinking through the 90-degree ply stack, which gradually occurs as it becomes energetically favorable to do so (in a manner similar to that described by He and Hutchinson [26]). Ultimately, the kinking crack grows towards the interface between the top of the 90-degree ply stack and a stack of 0-degree plies, resulting in onset of delamination growth along this interface, thereby completing the migration process. The relatively sudden exit of the kinked crack into the new 90/0 interface is indicative of the kinked crack having established a constant path of least resistance though the upper portion of the 90-degree ply stack (as evidenced by the linear appearance of the kink in this portion of the 90-degree ply stack), whereby the conditions that were energetically favorable for the kinking crack to turn resided locally at this 90/0 interface. The kink angle, Ω, is thus defined as the angle to the horizontal direction made by a line parallel to the linear portion of the kinked crack in the 90-degree ply stack, as illustrated in Figure 8. Further discussion regarding kink angles follows later in this section.

LOAD OFFSET, L=1.1a_0, 1.2a_0, and 1.3a_0

The force/displacement responses of an SCB specimen with load offsets equal to 1.1a_0, 1.2a_0, and 1.3a_0 are presented in Figures 9a, 9b, and 9c, respectively. Each case shown in the figures is typical of the other specimens tested at the three loading configurations. Specimens with the smallest load offset (L=1.1a_0) exhibited initial linear loading followed by stable delamination growth onset resulting in a small (approximately 1mm) amount of growth. This was followed by an unstable event that included unstable delamination growth along the 0/90 ply interface and migration, the onset of which ranged between 10-14mm past the load-application point, as illustrated in Figure 9a. The distance between the load application point and the onset of migration is denoted as Δ_k in Figure 9.

Specimens unloaded in a linear fashion ending with a residual displacement of approximately 0.12mm.

Specimens with load offsets equal to $1.2a_0$ and $1.3a_0$ behaved in a very similar manner to specimens whose load application was coincident with the PTFE insert front and exhibited the same sequence of event described previously for these specimens. In the case of the $L=1.2a_0$ offset specimens, delamination migration onset took place 7-10mm past the load-application point. Delamination migration onset in the $L=1.3a_0$ offset specimens took place 6-9mm past the load-application point.

The perceived path of the fracture events was similar in all specimens to those indicated in Figure 8.

EFFECT OF LOAD OFFSET ON MIGRATION

The plot in Figure 10a shows the distance from the load-application point at which delamination migration onset was observed (Δ_k) as a function of the load offset, L, normalized by the initial delamination length, a_0. Although the scatter in these data (between repeat specimens at each load offset) is quite high at a given load offset, the overall data tend to show that migration onset occurs closer to the load-application point as the load offset increases (migration onset in specimens with a load offset, $L=a_0$, was an exception to this rule). One possible explanation for this effect is that the mixed-mode loading conditions acting on the delamination front prior to migration are likely affected by the position of the load application point. This in turn will affect the apparent fracture toughness of the interface along which the delamination is growing and so will ultimately affect the location along the interface at which conditions favorable for kinking into the 90-degree ply stack will arise. An alternative explanation is that the speed of delamination growth may affect the fracture toughness of the interface and therefore affect the moment at which migration takes place. However, in all cases migration took place during seemingly similar unstable events, which tends to dilute delamination growth speed as a possible factor. A plot of kink angle versus load offset is given in Figure 10b. The scatter in these data is quite high and possibly masks any trend that may otherwise have been observed. The average kink angle was 61^o with a standard deviation of 9.8^o. This does suggest that kink angle was independent of load offset. Further analysis of kink angle is required before a more reliable conclusion can be offered. The data plotted in Figure 10 are also given in TABLE II.

Fractography

The fracture surfaces of a specimen from each of the four load offsets were inspected in a Philips XC30 scanning electron microscope. Micrographs taken of an SCB specimen with a load offset, $L=1.3a_0$, are presented in Figure 11. A total of ten images were taken, including five images along the central portion of the specimen, as illustrated on the sketch in Figure 11, and another five images near the specimen edge to the right of the central images. These later images where similar to their central counterparts and so only the central images are shown. Beginning with the micrograph taken near to the PTFE insert front, this region contains clean

looking 0-degree fibers with what appear to be shear hackles nested between a number of the fibers. This indicates a mixed mode-I/II form of loading as is expected along this 0/90 interface. The appearance of clean 0-degree fibers also indicate that the delamination is attempting to kink into the 0-degree ply but is ultimately prevented from doing so. As the delamination propagates to Region 2 in the specimen (see Figure 11), the fracture surface contains mostly imprints of 0-degree fibers. This indicates a transition of the propagating delamination away from the 0-degree ply. The surface of the beginning of the kinking crack in the 90-degree ply stack (Region 3) contains broken fibers, but overall the surface has a clean appearance. The fracture surface of the kinked crack in the middle of the 90-degree ply stack (Region 4) has clean looking broken fibers and regions of rotated shear hackles. The broken fibers indicate that kinking did not take place along a single plane, possibly indicating the fibers in this ply stack may not be aligned exactly along the 90-degree direction and parallel to one another. It is postulated that the generally clean looking surface is evidence of the kink being mode I dominated with regions of local mode III fracture, which occurs as 90-degree fibers deform and separate from one another. The final image (region 5) shows the beginning of the migrated delamination whose surface contains river lines that are indicative of mode I fracture [35].

To summarize, inspection of the specimen fracture surfaces indicates that delamination growth prior to migration takes place under a mixed mode-I/II form of loading. The kinked crack in the 90-degree ply stack appears to propagate under a predominantly mode-I form of loading, which is also the case for the migrated delamination. Images taken of fracture surfaces of all other specimens indicated a similar sequence of fracture events to that described above. However, additional microscopy will need to be performed to help evaluate the above summation and confirm that the observations from this fractographic analysis are consistent with specimens tested with load offsets of a_0, $1.1a_0$, and $1.2a_0$.

CONCLUDING REMARKS

A new test method has been developed for observing and documenting the migration of a propagating delamination. The test relies on the shear loading acting locally across the delamination for controlling the sequence of fracture events. The location in the specimen at which delamination migration onset occurred was found to be affected by the position of the load-application point (load offset). This is likely due to the change in load offset altering the mixed mode loading that drives the delamination prior to migration and thus changes the position at which migration onset becomes energetically favorable. Speed of delamination growth may also affect the fracture toughness of the interface and therefore affect the moment at which migration takes place. However, in all cases migration took place during seemingly similar unstable events, which tends to dilute delamination growth speed as a possible factor. Kink angle was found to be independent of load offset, although further analysis is required before a more concrete conclusion can be offered. A fractographic analysis of the fracture surfaces of the SCB specimens indicated that initial delamination is driven by a mixed mode-I/II form of loading while the crack that kinks into the 90-degree ply stack is largely driven by a mode-I

form of loading. The same mode-I dominated form of loading was observed in the migrated delamination. In general, use of this test allows for the observation of the growth of a delamination followed by migration of the delamination to another ply interface, and should thus provide a means for validating analyses aimed at simulating migration.

REFERENCES

1. Pipes, R. B. and N. J. Pagano. 1970. "Interlaminar Stresses in Composite Laminates Under Uniform Axial Extension," *Journal of Composite Materials*, 4:538-548.
2. Kima, J-K., D. B. MacKaya, and W-Y. Mai. 1993. "Drop-Weight Impact Damage Tolerance of CFRP with Rubber-Modified Epoxy Matrix," *Composites*, 24(6):485–494.
3. ASTM D5528-01 "Standard Test Method for Mode I Interlaminar Fracture Toughness of Unidirectional Fiber-Reinforced Polymer Matrix Composites," *2004 Annual Book of ASTM Standards,* Vol.15.03.
4. Davidson, B. D. and S. S. Teller. 2010. "Recommendations for an ASTM Standardized Test for Determining G_{IIc} of Unidirectional Laminated Polymeric Matrix Composites," *Journal of ASTM International*, 7(2):Paper ID JAI102619.
5. Brunner, A. J., B. R. K. Blackman, and P. Davies. 2008. "A Status Report on Delamination Resistance Testing of Polymer–Matrix Composites," *Engineering Fracture Mechanics*, 75:2779–2794.
6. Lee, S. M. 1993. "An Edge Crack Torsion Method for Mode III Delamination Fracture Testing," *Journal of Composites Technology and Research, JCTRER,* 15(3):193-201.
7. ASTM D6671M-04 "Standard Test Method for Mixed Mode I-Mode II Interlaminar Fracture Toughness of Unidirectional Fiber-Reinforced Polymer Matrix Composites," *2004 Annual Book of ASTM Standards,* Vol.15.03.
8. ASTM D6115-04 "Standard Test Method for Mode I Fatigue Delamination Growth Onset of Unidirectional Fiber-Reinforced Polymer Matrix Composites," *2004 Annual Book of ASTM Standards,* Vol.15.03.
9. O'Brien, T. K., W. M. Johnston, and G. J. Toland. 2010. "Mode II Interlaminar Fracture Toughness and Fatigue Characterizarion of a Graphite Epoxy Composite Material," *NASA Technical Memorandum*, NASA/TM-2010-216838.
10. Brunner, A. J. and P. Flueler. 2005. "Prospects in Fracture Mechanics of Engineering Laminates," *Engineering Fracture Mechanics*, 72(6):899–908.
11. Raju, I. S. and T. K. O'Brien. 2008. "Fracture Mechanics Concepts, Stress Fields, Strain Energy Release Rates, Delamination Initiation and Growth Criteria," in *Delamination Behavor of Composites*, E. Sridharan, ed. Woodhead Publishing Limited, pp. 3-27.
12. Rybicki, E. F. and M. F. Kanninen. 1977 "A Finite Element Calculation of Stress Intensity Factors by a Modified Crack-Closure Integral," *Engineering Fracture Mechanics*, 9:931-938.
13. Krueger, R. 2004 "Virtual Crack Closure Technique: History, Approach, and Application," *Applied Mechanics Reviews*, 57(2):109-143.
14. Dugdale, D. 1960. "Yielding of Steel Sheets Containing Slits," *Journal of the Mechanics and Physics*, 8:100–104.
15. Barenblatt, G. 1962. "The Mathematical Theory of Equilibrium Cracks in Brittle Fracture," *Advances in Applied Mechanics*, 7:55–129.
16. Camanho, P. P., C. G. Davila, and D. R. Ambur. 2001. "Numerical Simulation of Delamination Growth in Composite Materials," *NASA Technical Publication*, NASA-TP-211041.
17. Goyal, V. K., E. R. Johnson, and C. G. Davila. 2004. "Irreversible Constitutive Law for Modeling the Delamination Process Using Interfacial Surface Discontinuities," *Composite Structures*, 65:289-305.
18. Hull, D. and Y. B. Shi. 1993. "Damage Mechanisms Characterization in Composite Damage Tolerance Investigations," *Composite Structures*, 23(2):299-120.
19. Cantwell, W. J. and J. Morton. "The Impact Resistance of Composite Materials — A Review," *Composites*, 22(5):347–362.

20. Krueger, R., M. K. Cvitkovich, T. K. O'Brien, and P. J. Minguet. 2000. "Testing and Analysis of Composite Skin/Stringer Debonding under Multi-Axial Loading," *Journal of Composite Materials*, 34(15):1263-1300.
21. Owsley, G. S. 2000. "The Effect of Z-Fibre Reinforcement on Fatigue Properties of Stiffened Composite Panels," Presented at the 15th Technical Conference of the American Society for Composites, Texas, September 25-27, 2000.
22. Hallett, S. R., B. G. Green, W-G. Jiang, K. H. Cheung, and M. R. Wisnom. 2009. "The Open Hole Tensile Test: A Challenge for Virtual Testing of Composites," *International Journal of Fracture*, 158:169-181.
23. Belytschko, T., R. Gracie1, and G. Ventura. 2009. "A Review of Extended/Generalized Finite Element Methods for Material Modeling," *Modelling and Simulation in Materials Science and Engineering,* 17(4):1-24.
24. Yang, D. L. and B. Cox. 2009. "An Augmented Finite Element Method for Modeling Arbitrary Discontinuities in Composite Materials," *International Journal of Fracture*, 156(1):53-73.
25. Moës, N., J. Dolbow, and T. Belytschko. 1999. "A Finite Element Method for Crack Growth Without Remeshing," *International Journal for Numerical Methods in Engineering,* 46(1):131–150.
26. He, M-Y., and J. W. Hutchinson. 1989. "Kinking of A Crack Out of An Interface," *Journal of Applied Mechanics*, 56:270-278.
27. Wang., T. C. 1994. "Kinking of An Interface Crack Between Two Dissimilar Anisotropic Elastic Solids," *International Journal of Solids and Structures*, 31(5):629-641.
28. Canturri, C., E. S. Greenhalgh, S. T. Pinho, and J. Ankersen. "Delamination Growth Directionality and the Subsequent Migration Processes – The Key to Damage Tolerant Design," Presented at the 15th European Conference on Composite Materials, Venice, Italy, 24-28 June, 2012.
29. Jones, M. J. 1999. "Mechanics of Composite Materials," Taylor and Francis.
30. ABAQUS®/Standard Ver. 6.11 User's Manual, 2011.
31. O'Brien, T. K. and R. Krueger. 2003. "Analysis of Flexure Tests for Transverse Tensile Strength Characterization of Unidirectional Composites," *Journal of Composites Technology and Research, JCTRER*, 25:50-68.
32. Krueger, R., and T. K. O'Brien. 2001 "A Shell/3D Modeling Technique for the Analysis of Delaminated Composite Laminates," *Composites Part A: Applied Science and Manufacturing*, 32:25-44.
33. Raju, I. S., J. H. Crews Jr, and M. A. Aminpour. 1988. "Convergence of Strain Energy Release Rate Components for Edge-Delaminated Composite Laminates," *Engineering Fracture Mechanics*, 30(3):383-396.
34. Hexcel Corporation, 2007. "HexPly® 8552 Product Data Sheet," *http://hexcel.com*.
35. Greenhalgh, E.S. 2009. "Failure Analysis and Fractography of Polymer Composites," Woodhead Publishing In Materials.

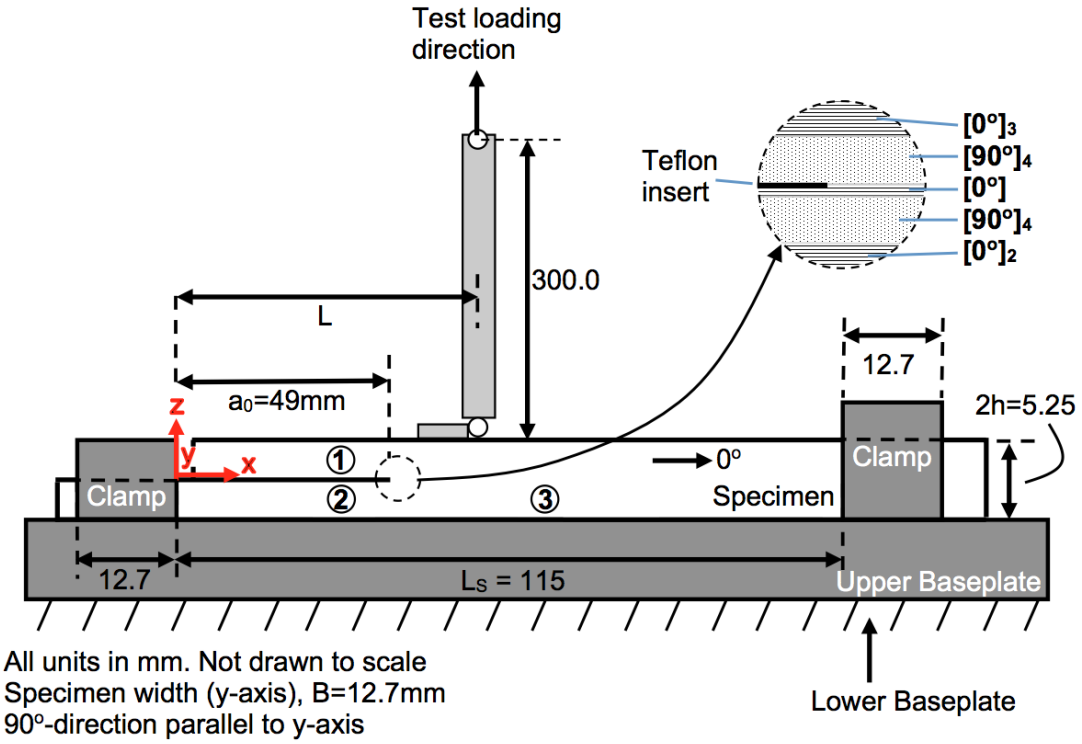

Figure 1. Schematic of SCB specimen.

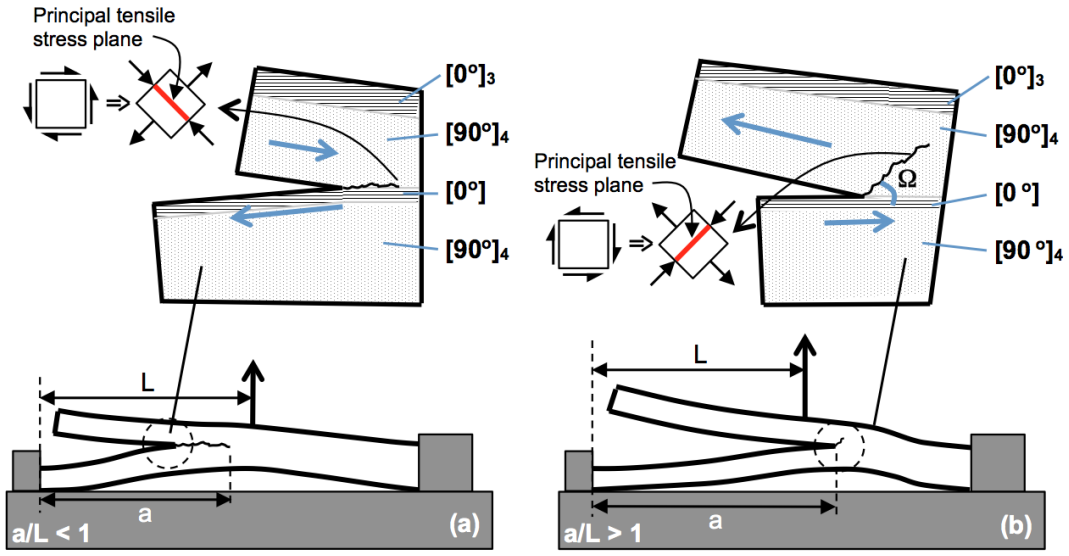

(a) Delamination extension (b) kink matrix crack extension

Figure 2. Shear stresses acting across the delamination front at different stages of growth.

Symmetric stacking sequence (condensed):
$\{[90_4/0_3/(90/0)_2]_s\}_s$

Symmetric stacking sequence (expanded):
$[90_4/0_3/(90/0)_{2s}/0_3/90_4/\ \mathbf{T}\ /90_4/\mathbf{0}/0/0/(90/0)_{2s}/0/0/\mathbf{0}/90_4]$

Actual SCB stacking sequence:
$[90_4/0_3/(90/0)_{2s}/0_3/90_4/\ \mathbf{T}\ /\mathbf{0}/90_4/0/0/(90/0)_{2s}/0/0/90_3/\mathbf{0}/90]$

Notes:
Sequence of plies: Left to right corresponds to upper to lower surfaces of the SCB specimen.
Teflon insert location indicated by letter, **T**.

Figure 3. Stacking sequence of SCB specimen.

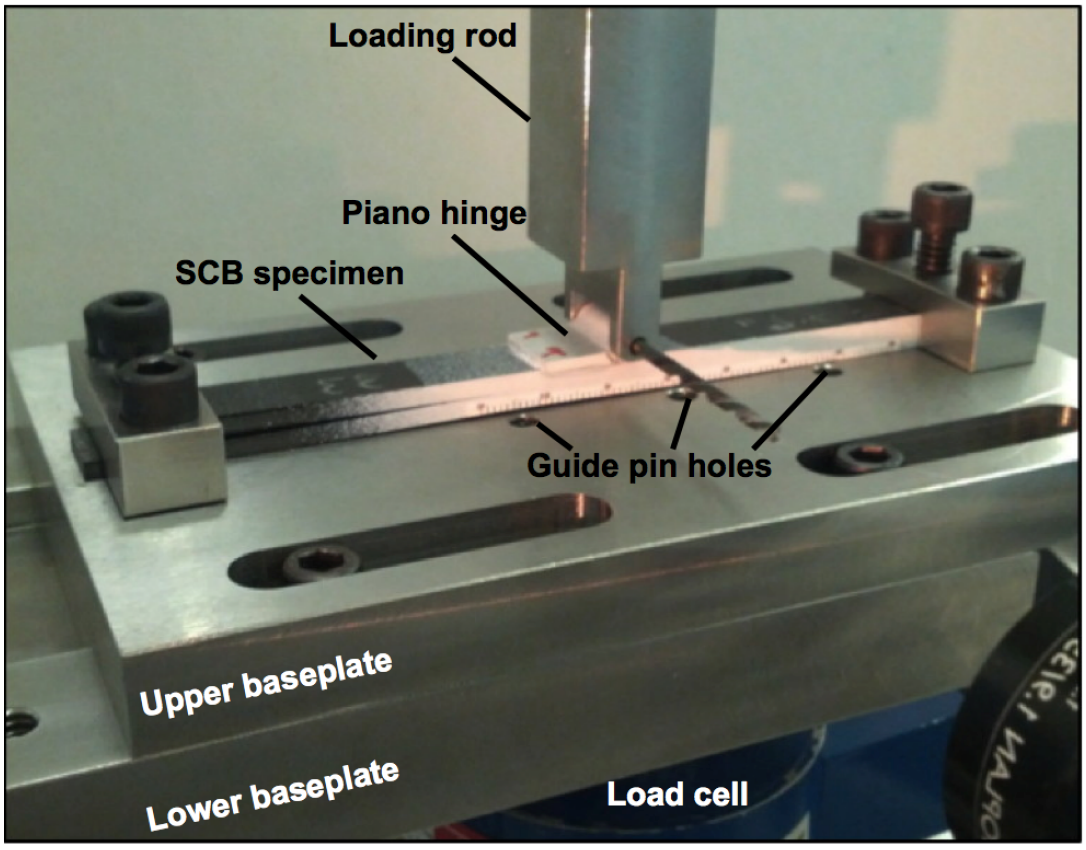

Figure 4. SCB test fixture with loaded specimen ($L=1.3a_0$).

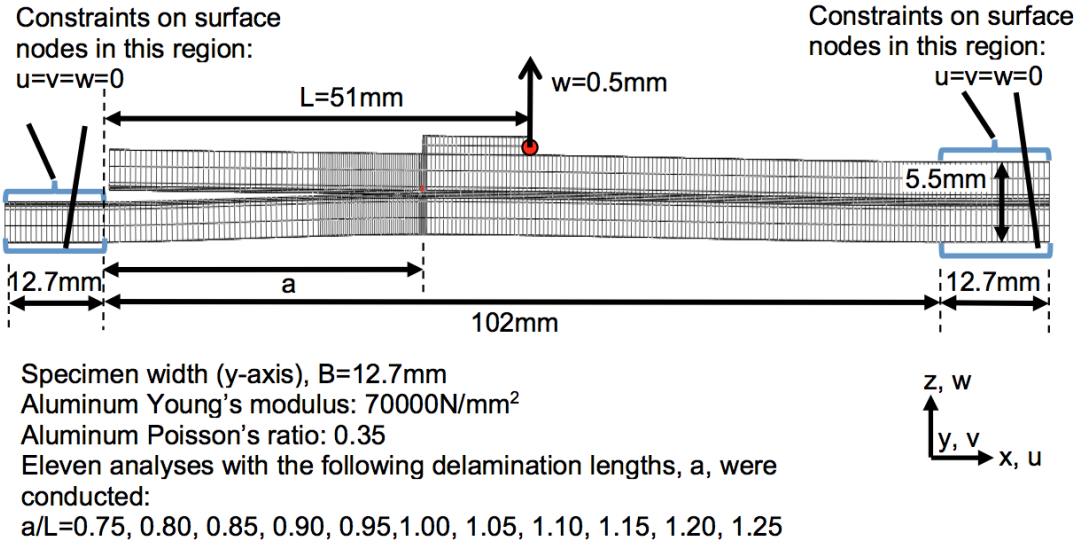

Figure 5. Finite element mesh of a SCB specimen (mesh along z-axis expanded to aid view).

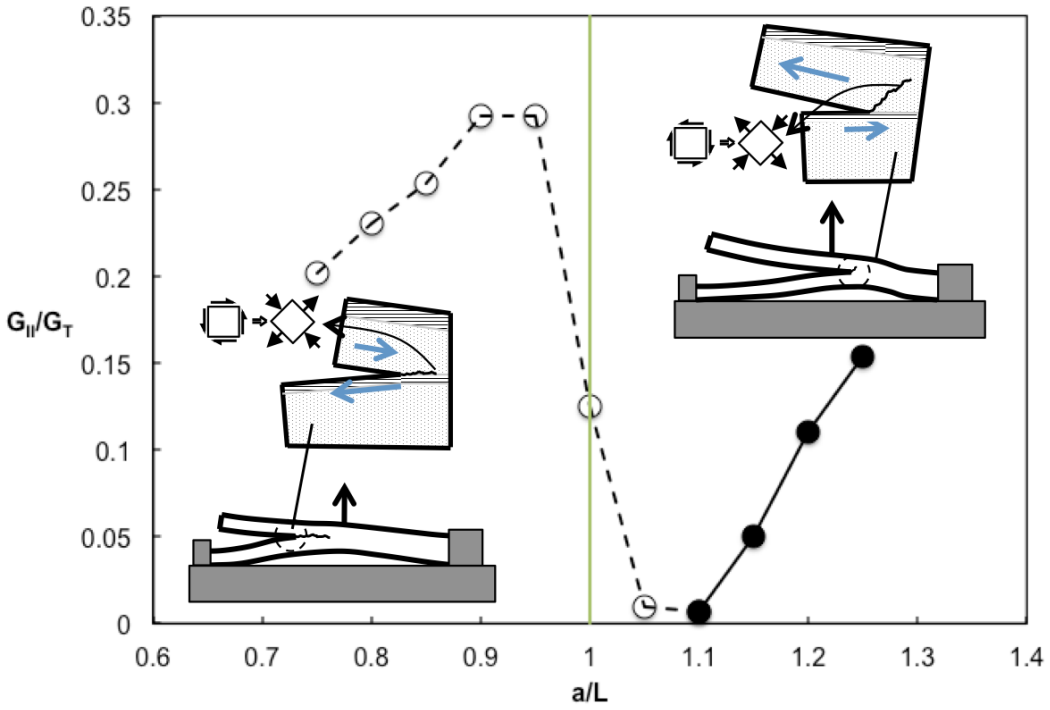

Figure 6. G_{II}/G_T as a function of normalized delamination length, a/L.

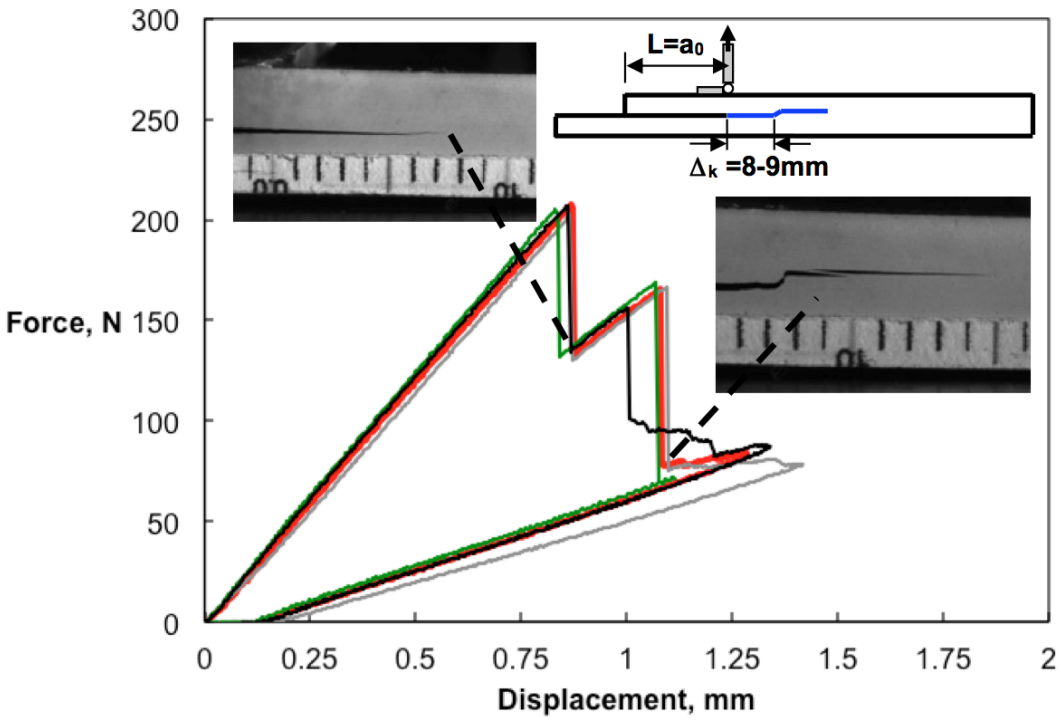

Figure 7. Force/displacement response of specimens loaded coindicentally with PTFE insert front.

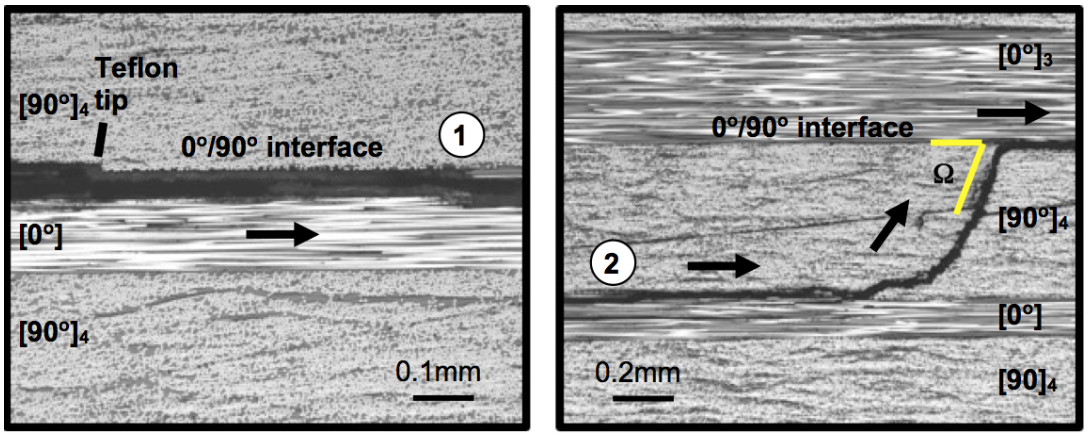

Figure 8. Micrographs of delamination onset and migration regions in a SCB specimen.

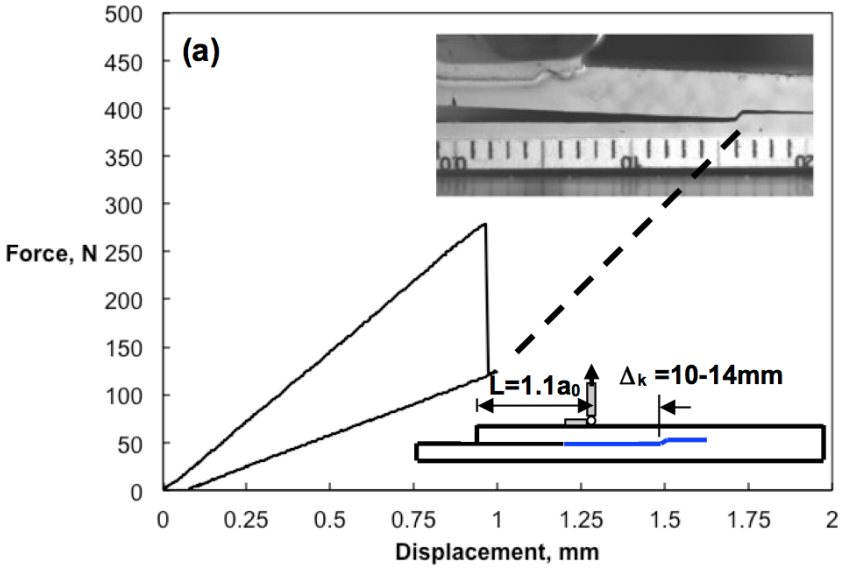
(a)
Force, N
Displacement, mm
L=1.1a0
Δk =10-14mm

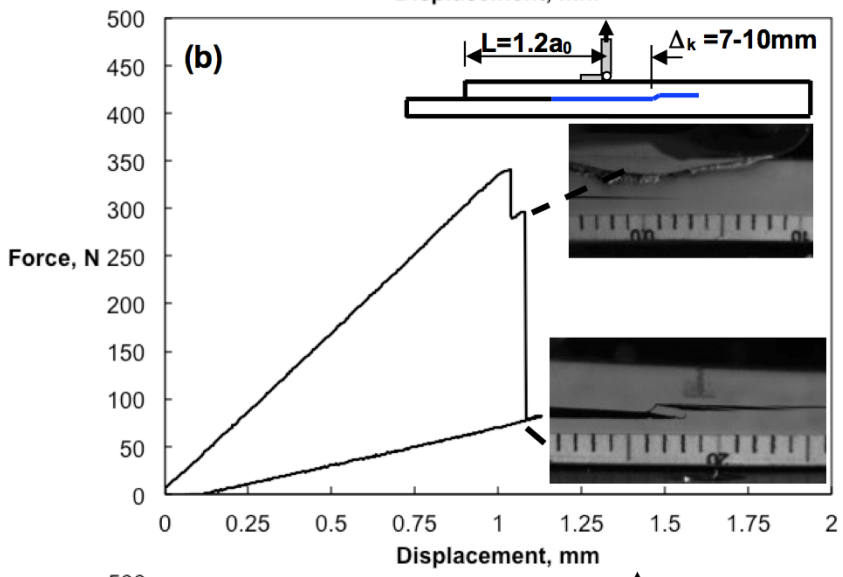
(b)
Force, N
Displacement, mm
L=1.2a0
Δk =7-10mm

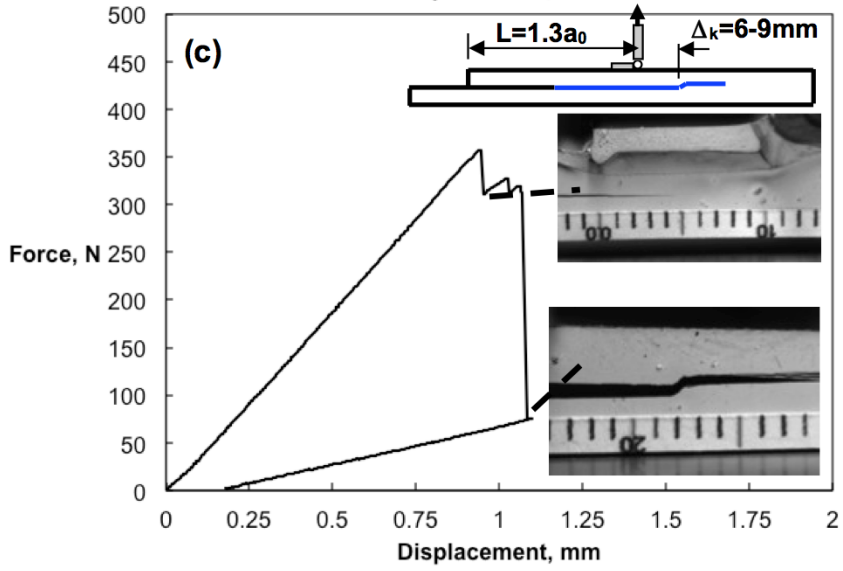
(c)
Force, N
Displacement, mm
L=1.3a0
Δk=6-9mm

Figure 9. Force/displacement response of SCB specimens (a) $L=1.1a_0$, (b) $L=1.2a_0$, (c) $L=1.3a_0$.

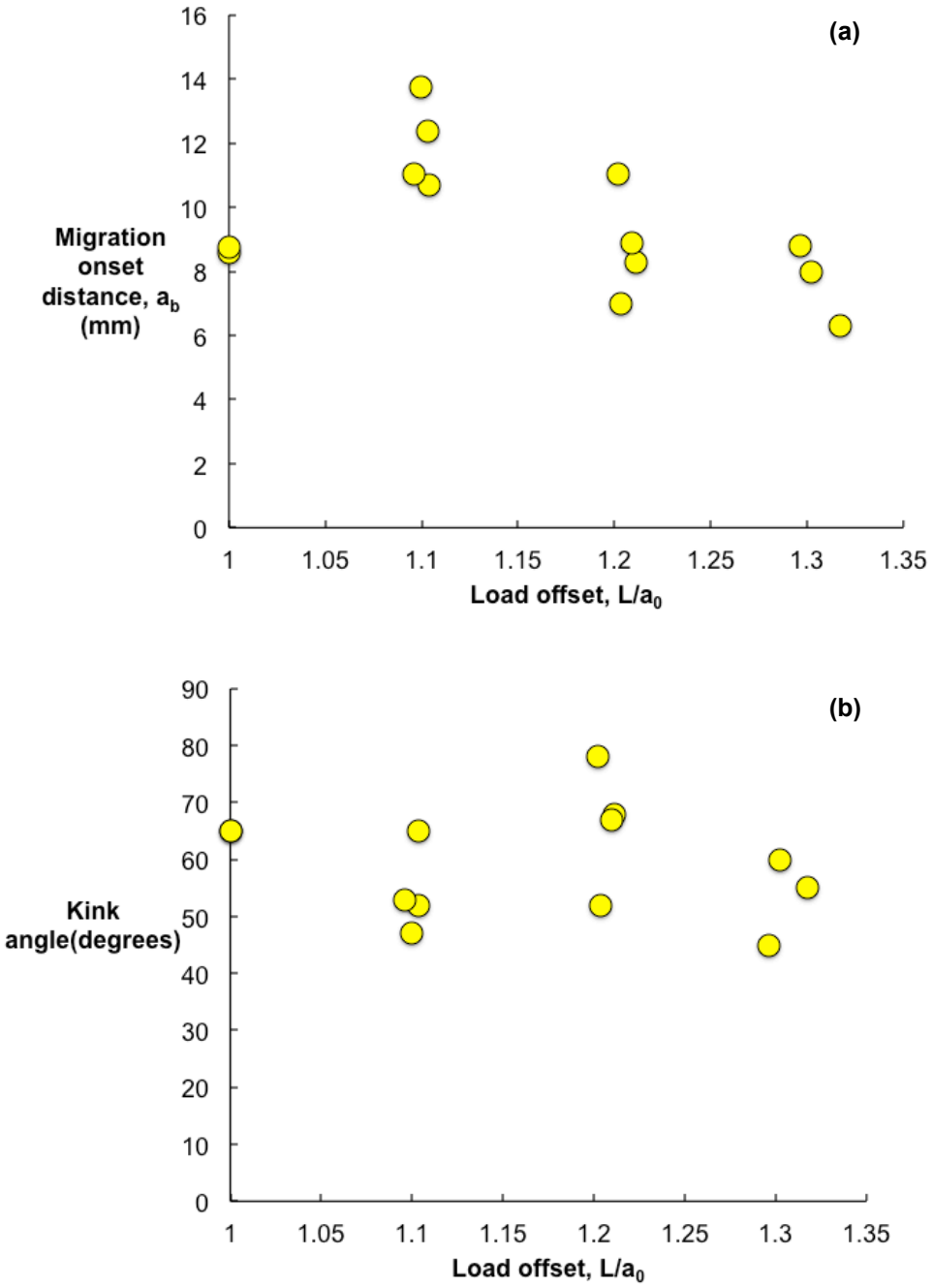

Figure 10. Effect of load-application offset, L, on, (a) location of delamination migration onset, (b) Kink angle.

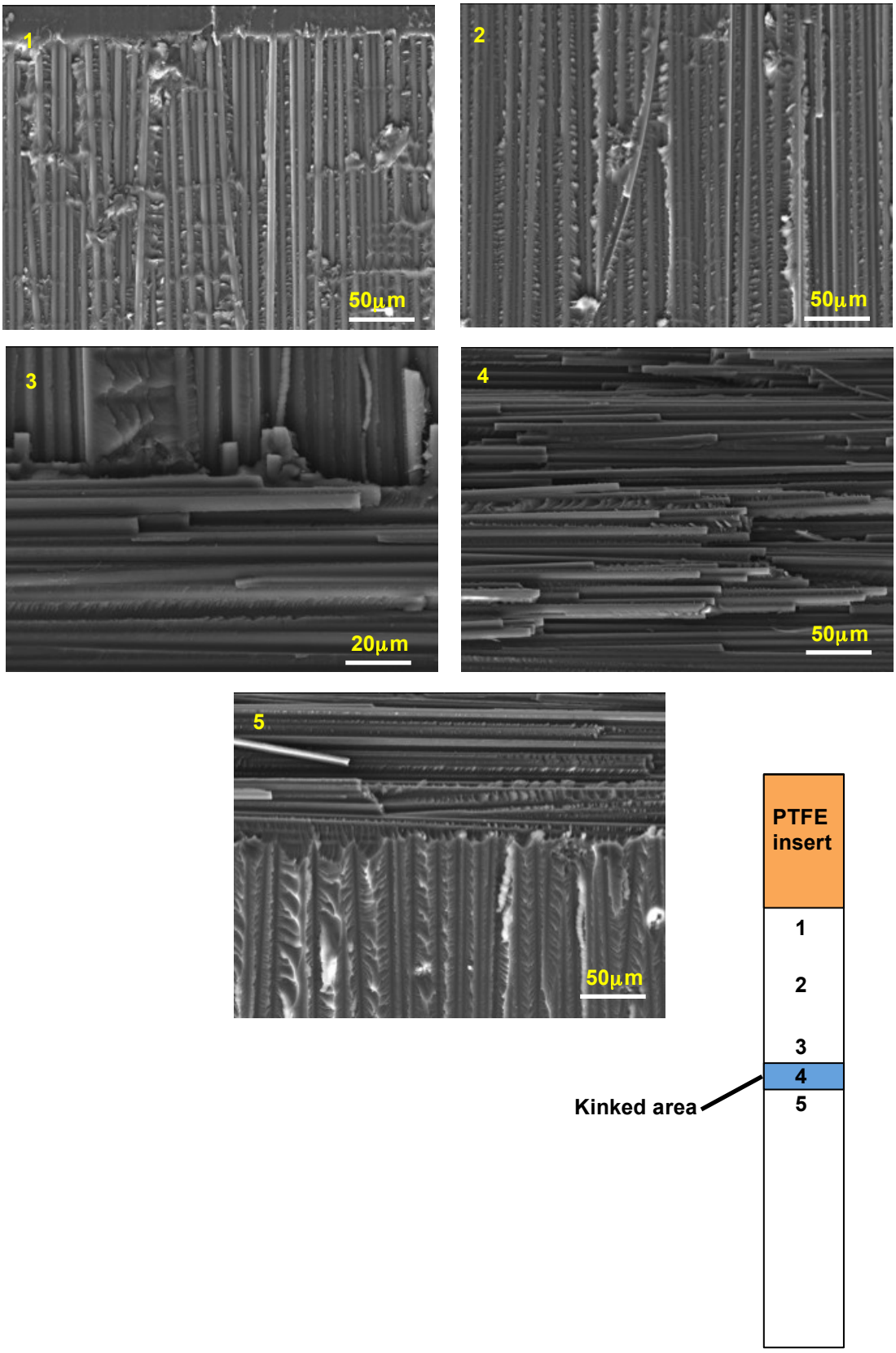

Figure 11. Scanning electron micrographs of SCB specimen fracture surfaces ($L=1.3a_0$)

TABLE I. MATERIAL PROPERTIES OF IM7/8552.

E_{11} = 161.0 GPa	E_{22} = 11.38 GPa	E_{33} = 11.38 GPa
ν_{12} = 0.32	ν_{13} = 0.32	ν_{23} = 0.436
G_{12} = 5.17 GPa	G_{13} = 5.17 GPa	G_{23} = 3.98 GPa
CTE (fiber direction) =-0.1E-6 1/K		
CTE (transverse direction) =31E-6 1/K		

TABLE II. EXPERIMENTAL DATA FROM SCB TESTS

Specimen	**Load offset L (mm)**	**Normalized load offset L/a_0**	**Relative* migration onset location, Δ_k (mm)**	**Kink angle Ω (degrees)**
SCB31	49.00	1.00	8.60	65
SCB35	48.55	0.99	8.75	74
SCB40	48.30	0.99	8.75	65
SCB42	49.00	1.00	9.22	68
SCB32	54.10	1.10	12.35	65
SCB36	53.90	1.10	10.70	52
SCB37	54.05	1.10	13.75	47
SCB39	53.70	1.10	11.05	53
SCB24	58.90	1.20	7.00	52
SCB26	58.95	1.20	8.90	67
SCB34	59.35	1.21	8.80	78
SCB41	59.25	1.21	8.30	68
SCB33	64.55	1.32	6.30	55
SCB38	63.55	1.30	8.80	45
SCB44	63.80	1.30	7.95	60

* Distance relative to the load-application point.